Effect of electron correlations on the excitation of neutral states of zinc in the autoionizing region: A photon emission study

S. A. Napier,[1] D. Cvejanović,[1,2] J. F. Williams,[1,2,*] and L. Pravica[1,2]
[1]*Centre for Atomic, Molecular and Surface Physics, School of Physics, University of Western Australia, Perth 6009, Australia*
[2]*ARC Centre for Antimatter-Matter Studies, School of Physics, University of Western Australia, Perth 6009, Australia*
(Received 11 June 2008; published 15 September 2008)

Electron impact excitation of the $4p\ ^{3,1}P_1$, $4d,5d,6d\ ^3D_{1,2,3}$, and $4d,5d\ ^1D_1$ states of the neutral zinc atom was studied by measuring photon decay intensities in the energy region of the $3d^9 4s^2 4p$ autoioionizing states. Two phenomena, both involving strong electron correlations and an active role of one of the $3d$ electrons in an intermediate scattering step, have been observed. The first is $3d$ core-excited negative-ion resonances, which dominate the energy region between 10.5 and 11.5 eV. The second is postcollision interaction (PCI) in the decay of autoionizing states which populates higher excited states at incident electron energies above 11.5 eV. The low energies of both the scattered and ejected electrons after near-threshold excitation of $3d^9 4s^2 4p$ autoionizing states enable a large transfer of orbital angular momentum, up to two units, by the PCI.

DOI: 10.1103/PhysRevA.78.032706 PACS number(s): 34.80.Dp

I. INTRODUCTION

This paper reports our continuing experimental studies of electron correlations in atoms, in particular how they affect the structure and scattering dynamics of zinc atoms.

The role of electron correlations in atomic structure is particularly prominent in zinc, which has an outermost ground-state electron configuration of $3d^{10}4s^2$. Zinc is situated in the periodic table at the point where electron-electron interactions between $3d$ and $4s$ electrons cause a departure from the general electron configuration energy ordering expected from a central field approximation. If the electronic structure of an atom is considered as an admixture of configurations, with independent particle configurations of given n and l as a starting point, but also with continuum and multiply excited configurations, then it is this admixture which describes the correlations. This basic approach has underpinned previous studies [1] in neon in which incident spin-polarized electrons enabled observation and interpretation of the angular momentum parameters.

The present observations indicate that electron correlations in Zn become pronounced upon the excitation of a $3d$ electron and have a significant influence on electron scattering. Experimental evidence, from both photon [2,3] and electron impact studies [4–6], indicates that the excitation probability for some $3d^9 4s^2 4p$ autoionizing states is comparable over a range of energies and scattering angles to those of $3d^{10}4snl$ states which lie below the ionization threshold. These states have also been shown by the structure calculations of Mansfield [7] to have a strong mixing of states with different orbital angular momentum, spin, and electron configuration. For example, the observed energy ordering of the optically allowed $3d^9 4s^2 4p\ ^3P_1$, $^3D_1$, and $^1P_1$ states [2] could be obtained only if perturbation mixing with the $3d^{10}4s4p$ configuration was included in the theory. Thus, it is reasonable to expect that the $3d^9 4s^2 4p$ states of zinc provide fertile ground for the exploration of electron correlations.

In the present measurements, the target zinc atom is perturbed with an incident electron which participates in the subsequent correlations. As a result, two different types of effects, both dependent on the electron correlations which influence structure and the scattering dynamics, are observed here. The first is the formation and decay of negative-ion resonances, which result when the scattered electron is temporarily bound to the atom to form a complex which then decays to a neutral bound state plus an unbound electron. The second is the postcollision interaction (PCI), where scattered and ejected electrons resulting from the excitation and decay of an autoionizing state exchange energy via the Coulomb interaction, which modifies their trajectories and final energies. Of the many possibilities of PCI [8], the one observed here involves the recapture of the lower-energy scattered electron to form a neutral state lying below the ionization threshold. Both effects are observed here as interference in the direct excitation of neutral states in the vicinity of the $3d^9 4s^2 4p$ state thresholds.

The experimental and theoretical work on negative-ion resonances in zinc has been reviewed [9,10]. The majority of information is limited to negative-ion resonances below the ionization threshold and, with exception of two studies [6,10], were observed in optical excitation functions [11–13] or transmission experiments [10,14]. Optical excitation functions [11–13] for the $4p\ ^3P_1$, $5s\ ^3S_1$, $4d,5d,6d\ ^1D_2$, and $4d,5d\ ^3D_{1,2,3}$ states above the ionization threshold show structures with moderate detail. Stokes polarization parameter measurements observing $4d\ ^1D_1$ state decay photons emitted after excitation by spin-polarized electrons [15] have shown the role of spin-orbit and exchange interactions in the resonances above the ionization threshold. Existing theoretical negative-ion resonance calculations using the B-spline R-matrix (BSRM) method [16] are limited to below 8.5 eV. The standard approach based on the frozen core model is inadequate for the modeling of negative-ion resonances with a hole in the $3d$ orbital. So far, zinc negative-ion resonances associated with the excitation of a $3d$ electron have not been modeled.

PCI can be identified because it characteristically affects the excitation of higher-lying states, and PCI structures

*jfw@cyllene.uwa.edu.au

present in nL_J^{2S+1} state excitation functions shift upwards in energy with increasing n. The effect has been observed and analyzed in detail for the excitation of autoionizing states just above their threshold [8,17] and for electron scattering from helium. Models of these PCI effects have been presented by King *et al.* [8], Barker and Berry [18], Morgenstern *et al.* [19], van der Burgt *et al.* [20], and van de Water and Heideman [21]. In the case of the $3d^9 4s^2 4p$ autoionizing states of zinc excited within 2.5 eV of the threshold, both the scattered and ejected electrons are slow, spend a relatively long time in the field of the Zn^+ ion, and so resemble two Wannier electrons. A similar situation, for an excited ion with a vacancy in an inner shell, was described by Kuchiev [22]. As a consequence, the probability for both the exchange of energy and the exchange of angular momentum is enhanced.

We present here an investigation of the negative ion resonance and PCI effects on the photon excitation functions of the $4p\ ^{3,1}P_1$, $4d,5d,6d\ ^3D_{1,2,3}$, and $4d,5d\ ^1D_1$ states. Investigating the excitation of a diverse range of states exploited the n, L-, and S-dependent behavior of the correlation effects and permitted different contributions to the complex interference structures to be observed. The negative-ion resonances and PCI have been classified in terms of the energy at which they appear and the excitation channels in which they have been observed.

II. EXPERIMENT

Photon excitation functions were measured using a crossed-beams, electron impact spectrometer discussed in our previous publication [23]. Briefly, electrons emitted from a V-shaped cathode were energy selected using a 127° cylindrical energy selector and then crossed with an atomic zinc beam emanating from a thermally heated oven. Photons emitted in a direction perpendicular to the electron beam were collected by a lens, wavelength selected using an interference filter, and detected by a cooled photomultiplier tube. The energy spread in the incident beam was typically 80 meV except for the study of the $5d\ ^1D_{1,2,3}$ and $6d\ ^3D_{1,2,3}$ states where it was increased to 120 meV, and hence the incident current was increased, to compensate for the low signal detected for these states. The incident beam energy was subject to drifts due to changes in surface potentials on the order of 40 meV over the time needed to obtain individual excitation functions.

The energy scale was calibrated by detecting 636 nm photons from decay of the $4d\ ^1D_2$ state as the incident energy was scanned across the steplike threshold of this state. The experimental intensities were fitted to BSRM calculations of the $4d\ ^1D_2$ integral cross section convoluted with a Gaussian apparatus function [16]. This procedure determined the energy spread in the incident beam and the energy offset to an accuracy of 10 meV. Calibrations were performed before and after each scan, and then averaged to account for energy drifts. The total energy uncertainty in the present experiment due to the calibration and energy drifts is 30 meV.

III. RESULTS

Photon excitation functions for the $4p\ ^3P_1$, $4p\ ^1P_1$, $4d,5d,6d\ ^3D_{1,2,3}$, and $4d,5d\ ^1D_{1,2,3}$ states of zinc are shown in Figs. 1–4. These measurements, taken with an incident energy ranging between the ionization threshold at 9.394 eV and 17 eV, show significant effects due to negative ion resonances and PCI. All the excitation functions presented are affected by cascades throughout the energy region studied. The data presentation is organized to facilitate a comparison between how different structures affect the excitation of states with different n, L, and S quantum numbers, and thus illustrate the angular momentum and binding energy dependence of the observed electron correlation effects.

Negative-ion resonances and PCI structures were isolated by subtracting a least-squares polynomial fit to the slowly varying background contribution to the observed excitation functions. This estimated background is shown as a solid line in Figs. 1–4 along with the isolated structure contributions as a percentage of the interpolated background. By subtracting a background, the relative sizes of the various resonance and PCI structures as well as details of their shape become more apparent. It is particularly important to see clearly the finer details in the case of unresolved resonances, as this helps to identify the presence of multiple-resonance and possible cascade and interference effects. A subtracted background also allows the onset of PCI structures to be seen more clearly, which is important for analysis.

The energies of observed features are shown in Tables I–III. Unless otherwise indicated, the quoted energies correspond to peaks in the excitation functions, the energy positions of which were estimated by a peak fit to the top parts of each feature. The total uncertainty, which included the calibration uncertainty and uncertainty due to energy drifts and the peak fit, are indicated for each feature in the table.

Negative-ion resonances are labeled here with letters to associate structures which appear, within the experimental uncertainties, at the same energy irrespective of the neutral state observed. However, there was some difficulty in establishing precise resonance energies and associating structures because the present resolution was insufficient to resolve completely the closely spaced observed features, which also seem to have a large natural width. Consequently, we see composite peaks appearing as unresolved doublets or triplets and causing modifications to the expected single-resonance profile. The present experiment indicates the existence of at least six resonances, which can be resolved partly because of their different decay channel branching ratios. Three resonance groups with closely spaced components were observed, so the letters a, b, and c were used to identify members of the same group and dashes, for example c, c', and c'', used to distinguish the closely spaced components.

The structures observed in $nd\ ^{3,1}D$ state excitation functions, and identified as PCI effects because of their n dependence, are labeled with numbers in order of increasing energy positions. The number is preceded by the letter T for features observed in $nd\ ^3D$ excitation functions and the letter S for features observed in $nd\ ^1D$ excitation functions.

A. $4p\ ^{3,1}P_1$ states

Photon excitation functions and inset percentage resonance contributions for the $4p\ ^{3,1}P_1$ states in the energy re-

gion from 10.3 to 12.8 eV are shown in Figs. 1(a) and 1(b), and a resonance observed in the $4p\ ^1P_1$ state excitation function above 16 eV is shown in Fig. 2. These two states are the lowest excited states of zinc, with the $4p\ ^3P_{0,1,2}$ state having excitation thresholds at 4.006 ($J=0$), 4.030 ($J=1$), and 4.078 eV ($J=2$) and the $4p\ ^1P_1$ state having an excitation threshold of 5.796 eV. The singlet state decays by emission of 214 nm photons via the transition $4p\ ^1P_1 \rightarrow 4s^2\ ^1S_0$. The $4p\ ^3P_{0,1,2}$ state is metastable, and only the $J=1$ component decays radiatively by emission of 308 nm photons via the $4p\ ^3P_1 \rightarrow 4s^2\ ^1S_0$ transition. As discussed in detail by Napier *et al.* [23], the interference filter used to investigate $4p\ ^3P_1$ also transmitted 304 nm photons from the $6s\ ^3S_1 \rightarrow 4p\ ^3P_{0,1,2}$ transition. However, since the cross sections of higher states, including $6s\ ^3S_1$, should be considerably smaller than those of $4p\ ^{3,1}P$, 304 nm photon and cascade contributions from individual states should be negligible. On the other hand, a cumulative contribution from cascading states with similar resonance paterns—for example, cascades from the $nd\ ^3D$ states discussed in Sec. III B—may be significant.

The $4p\ ^3P_1$ excitation function shown in Fig. 1(a) contains three strong resonance structures, resonance a at 10.76 eV, b' at 11.09 eV, and c'' at 11.42 eV, each with a height close to 30% of the interpolated background. Shoulders on the 11.42 eV peak at 11.34 eV and 11.66 eV indicate possible contributions from other resonance states, and for example a resonance peak is clearly seen at 11.31 eV in the $4d\ ^1D_1$ excitation function shown in Figs. 4(a) and 4(b). Compared to differential electron excitation functions for the $4p\ ^3P_{0,1,2}$ state [6], the lower two peaks observed here have a much larger intensity relative to the 11.42 eV peak. This may be explained by the fact that the fine structure levels ($J=0,1,2$) are all detected in the electron measurements, while only photons from the $J=1$ level are detected in the present photon measurements. Also, the electron measurements will be unaffected by cascades.

The $4p\ ^1P_1$ state excitation function from 10.5 to 12.5 eV is shown in Fig. 1(b) and from 15 to 17 eV in Fig. 2. There are fewer resonances observed in the 10.5 to 12.5 eV energy region than for $4p\ ^3P_1$, and the height of the largest peak is only 8% of the interpolated background. The feature a is present only as a shoulder at 10.74 eV, the feature b is present at 11.00 eV, and the feature c is present at 11.22 eV. The significant dip in intensity near 11.5 eV may possibly be related to the 11.42 eV resonance c'' or perhaps may simply be the trailing edge of a resonance profile. A comparison with the $4p\ ^3P_1$ excitation function suggests that, of the closely spaced components of the b and c groups, the lower-energy resonances decay predominantly into the singlet state and the higher-energy resonances decay predominantly into the triplet state.

Figure 2 shows a small isolated resonance with a size equal to 1.3% of the interpolated background. Since the resonance was isolated, a Fano profile was fitted using the method described in [23], which yielded a resonance energy of 16.16 eV and an apparent width of $\Gamma=460$ meV. This feature has previously been observed in $5d,6d\ ^1D_2$ excitation functions [13] and is presented here for completeness. As

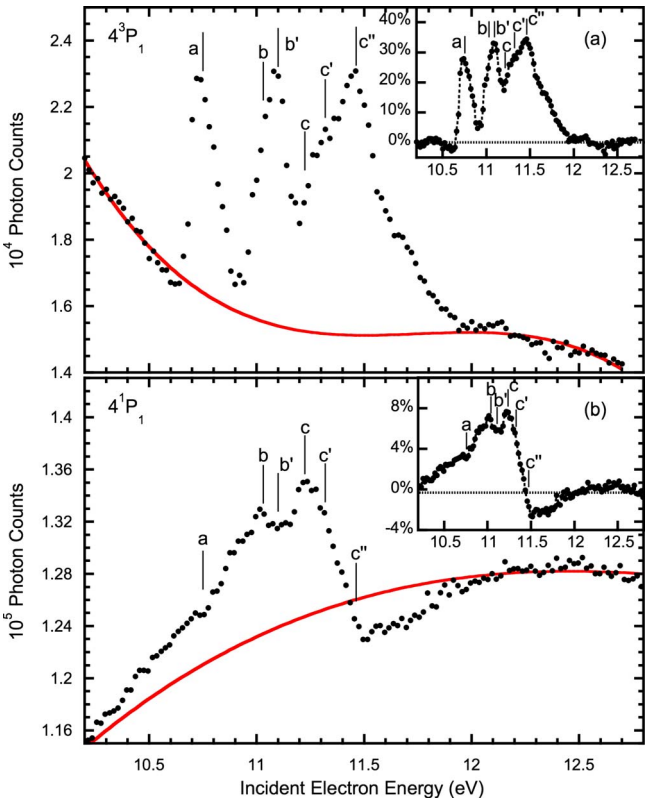

FIG. 1. (Color online) The photon excitation functions for the (a) $4p\ ^3P_1$ and (b) $4p\ ^1P_1$ states of zinc: (●) present data, (solid line) estimated smoothly varying background. Inset: (dot-dashed line) resonance contributions as a percentage of the total signal. Vertical bars labeled by letters indicate the average energy of structures presented in Table I.

only a very limited study of this resonance is presented here, no attempt at classification will be made. However, we note that all states within 0.5 eV of the resonance have a $3d^9 4s^2 np$ or $3d^9 4s^2 nf$ configuration [24]. Also, this resonance will not be included in Table I and the discussion since it is unrelated to all other resonances investigated here.

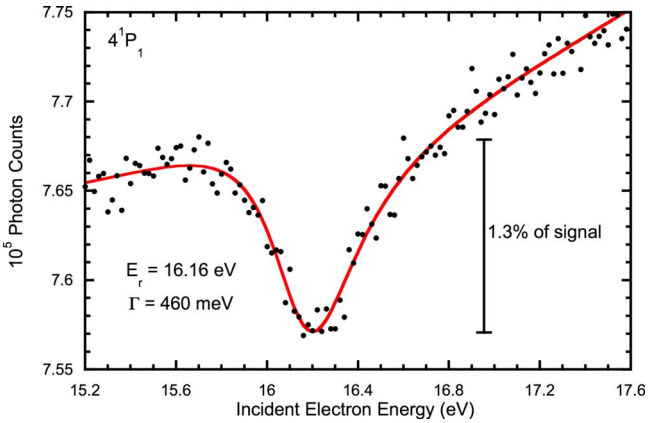

FIG. 2. (Color online) The photon excitation function for the $4p\ ^1P_1$ near 16 eV: (●) present data, (solid line) a combined polynomial background and Fano profile fit to the resonance structure which obtained the resonance energy and width displayed.

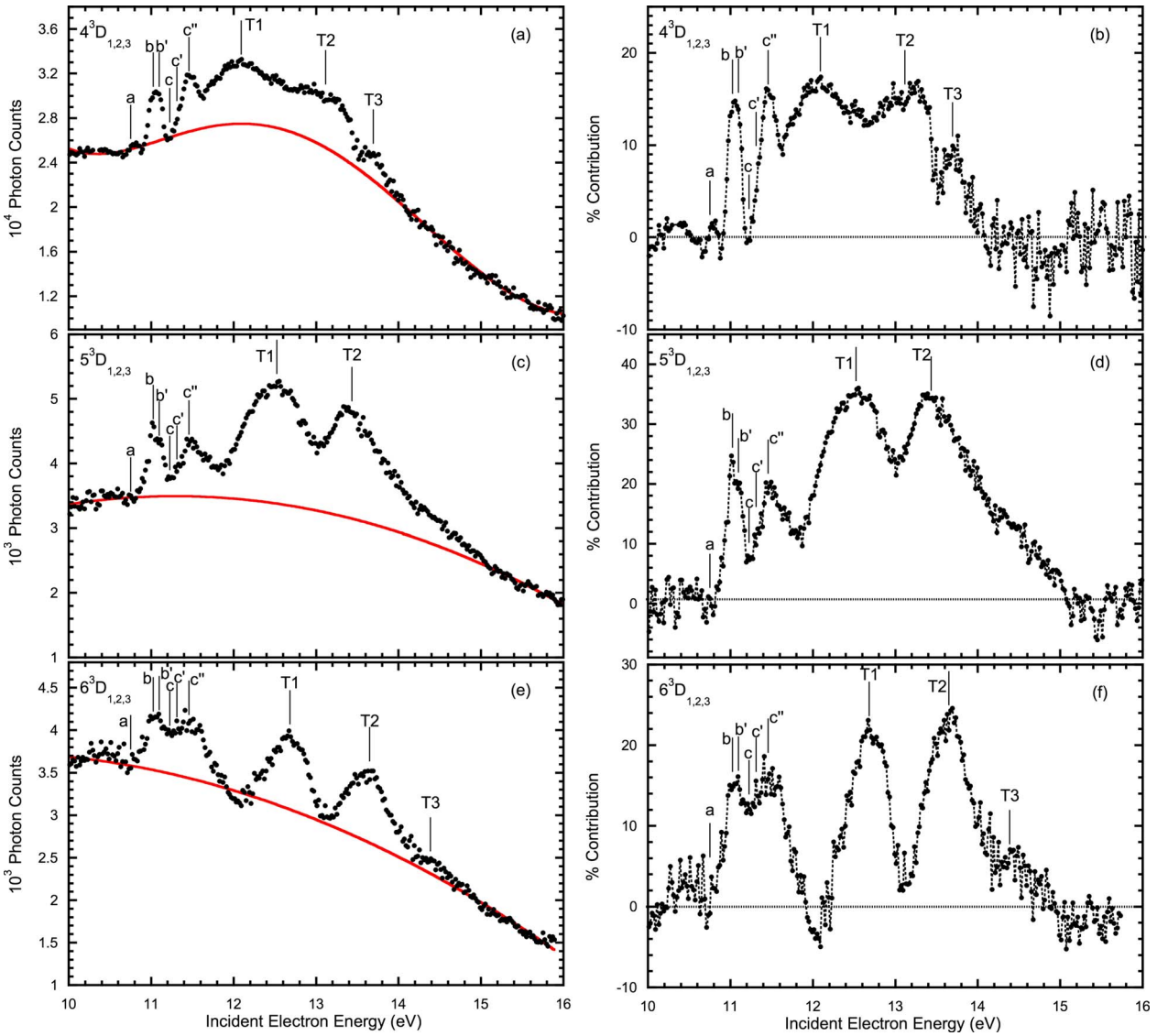

FIG. 3. (Color online) The photon excitation functions and resonance and PCI structure contributions as a percentage of the total signal for (a) and (b) $4d\,^3D_{1,2,3}$, (c) and (d) $5d\,^3D_{1,2,3}$, (e) and (f) $6d\,^3D_{1,2,3}$: (●) present data, (solid line) estimated smoothly varying background, and (dot-dashed line) the percentage resonance and PCI structure contribution to the data. Vertical bars labeled by letters indicate the average energy of structures presented in Tables I and II.

TABLE I. Energies of resonance structures observed in photon excitation functions for the $4p\,^{3,1}P_1$, $4d,4d,6d\,^3D_{1,2,3}$, and $4d,5d\,^1D_2$ states. The total energy uncertainty due to energy calibration, energy drifts, and the peak fitting is indicated for each structure. The letters in the leftmost column refer to the resonance labels used to identify negative ion resonances throughout this paper. Data from previous photon excitation functions [13] are presented for comparison. All energies are in units of eV.

Res.	Present experiment							
Label	$4p\,^3P_1$	$4p\,^3P_1$	$4d\,^3D_{1,2,3}$	$5d\,^3D_{1,2,3}$	$6d\,^3D_{1,2,3}$	$4d\,^1D_2$	$5d\,^1D_2$	Ref. [13]
a	10.76 ± 0.04	10.74 ± 0.05[a]	10.79 ± 0.04	10.75 ± 0.05[b]	10.73 ± 0.05[b]			
b		11.00 ± 0.04	11.05 ± 0.04	11.02 ± 0.04		11.01 ± 0.05[a]		
b′	11.09 ± 0.04			11.14 ± 0.04	11.08 ± 0.04	11.10 ± 0.04	11.06 ± 0.05	11.11
c		11.22 ± 0.04						
c′	11.34 ± 0.05[a]					11.31 ± 0.04	11.29 ± 0.05	11.30
c″	11.42 ± 0.04		11.48 ± 0.04	11.50 ± 0.04	11.44 ± 0.04			

[a]Appears as a shoulder.
[b]Appears as a small dip.

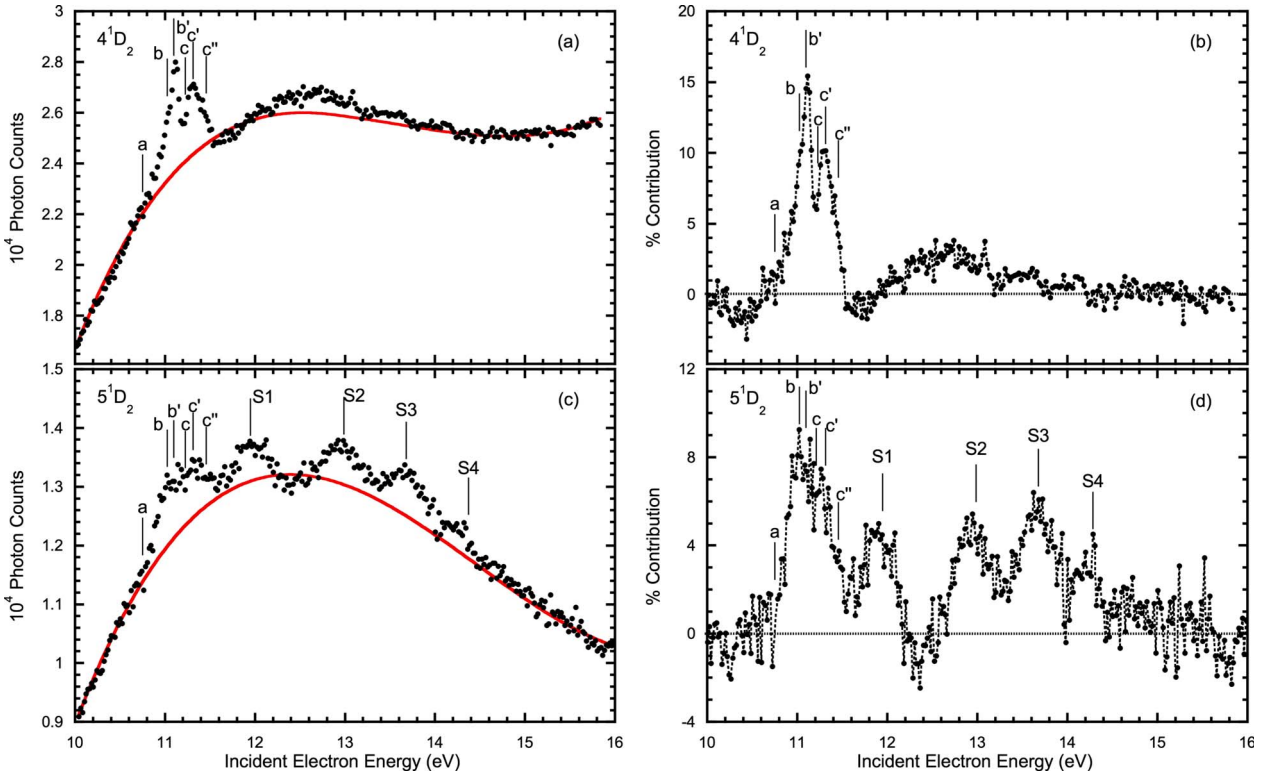

FIG. 4. (Color online) The photon excitation function and resonance and PCI structure contributions as a percentage of the total signal for (a) and (b) $4d\,^1D_2$, (c) and (d) $5d\,^1D_2$: (●) present data, (solid line) estimated smoothly varying background, and (dot-dashed line) the percentage resonance and PCI structure contribution to the data. Vertical bars labeled by letters indicate the average energy of structures presented in Tables I and III.

There are no structures in the $4p\,^{3,1}P_1$ excitation functions which can be associated clearly with PCI effects. This is expected since the PCI affects predominantly the excitation of higher-energy, higher-n neutral states [25].

B. $4d,5d,6d\,^3D_{1,2,3}$ states

The photon excitation functions for the $4d,5d,6d\,^3D_{1,2,3}$ states in the energy region between 10 and 16 eV are shown in Figs. 3(a), 3(c), and 3(e), alongside percentage contributions from negative ion resonances and PCI structures in Figs. 3(b), 3(d), and 3(f). The threshold energies of these states are 7.783, 8.503, and 8.829 eV for $n=4$, 5, and 6, respectively. The three observed transitions $4d,5d,6d\,^3D_{1,2,3}\rightarrow 4p\,^3P_{0,1,2}$ each give rise to six closeley spaced spectral lines which were transmitted with different efficiencies as discussed in [23]. The interference filters had maximum transmission at 334 nm for $4d\,^3D_{1,2,3}$, 283 nm for $5^3D_{1,2,3}$, and 262 nm for $6^3D_{1,2,3}$.

TABLE II. Energies of peaks observed in photon excitation functions for the $4d,5d,6d\,^3D_{1,2,3}$ states attributed to PCI. The total energy uncertainty due to energy calibration, energy drifts, and the peak fitting is indicated for each structure. The labels $T1$, $T2$, and $T3$ are used to identify the individual peaks throughout this paper. All energies are in units of eV.

	PCI structures		
Excited state	T1	T2	T3
$4d\,^3D_{1,2,3}$	12.10 ± 0.04	13.12 ± 0.05	13.69 ± 0.04
$5d\,^3D_{1,2,3}$	12.53 ± 0.04	13.44 ± 0.05	
$6d\,^3D_{1,2,3}$	12.68 ± 0.04	13.65 ± 0.05	14.38 ± 0.07

As can be seen in Fig. 3 at least four negative-ion resonances affect the excitation functions below 12 eV. Resonance a is clearly visible as a peak at 10.79 eV for $n=4$, but is a small dip for the other two states. For the b structure group, favorable relative resonance contributions to the $5d\,^3D_{1,2,3}$ excitation function and a lack of drifts during the scan led to a doublet structure, with peaks b at 11.03 eV and b' at 11.11 eV, being resolved. The b group doublet is not resolved in the $4d\,^3D_{1,2,3}$ excitation function; however, the $4d\,^3D_{1,2,3}$ spectrum peak at 11.05 eV, in Figs. 3(a) and 3(b), lies between the $5d\,^3D_{1,2,3}$ resonance peaks b and b' in Figs. 3(c) and 3(d). This suggests that two unresolved resonances contribute to the $4d\,^3D_{1,2,3}$ b structure. This could also be true of the $6d\,^3D_{1,2,3}$ spectrum structure at 11.08 eV, marked b' in Figs. 3(e) and 3(f). The third structure, marked c'' in Figs. 3(a)–3(c) is observed around 11.47 eV in all three states. This peak appears in all ^3D spectra as a relatively broad and complex peak, suggesting the presence of the c and c' resonance observed in the other excitation channels.

At energies above 11.5 eV a series of broad enhancements are observed in all ^3D spectra which, because of their upward energy shift with increasing n of the state observed, have been attributed to PCI. As shown in Figs. 3(b), 3(d), and 3(f), two peaks $T1$ and $T2$ are resolved clearly in all

TABLE III. Energies of peaks observed in photon excitation functions for the $5d\ ^1D_2$ state possibly due to PCI. The total energy uncertainty due to energy calibration, energy drifts, and the peak fitting is indicated for each structure. The labels *S*1, *S*2, *S*3, and *S*4 are used to identify the individual peaks throughout this paper. Previously published peak energies for the $5d\ ^1D$ state photon excitation function [13] are presented for comparison. All energies are in units of eV.

	PCI structures			
Excited state	S1	S2	S3	S4
$5d\ ^1D_2$ (present)	11.94 ± 0.04	12.98 ± 0.04	13.69 ± 0.05	14.24 ± 0.04
$5d\ ^1D_2$ (Shpenik *et al.*)	12.03	13.07	13.72	

spectra and have heights up to around 30% of the interpolated background. A third peak *T*3 is less well resolved for the $4d\ ^3D_{1,2,3}$ and $6d\ ^3D_{1,2,3}$ states, and not resolved at all for the $5d\ ^3D_{1,2,3}$ state. The estimated position of the peak for each structure is shown in Table II. As *n* of the observed state increases, the peaks not only shift upward in energy, but also appear to get narrower. As a result, the PCI structures change from broad enhancements overlapping each other and the ~11-eV resonances in the $4d\ ^3D_{1,2,3}$ spectrum to peaks well separated from the resonances and each other in the $6d\ ^3D_{1,2,3}$ spectrum.

C. $4d,5d\ ^1D_2$ states

The photon excitation functions for the $4d,5d\ ^1D_2$ states in the energy region between 10 and 16 eV are shown in Figs. 4(a) and 4(c) alongside percentage contributions from negative ion resonances and PCI structures in Figs. 4(b) and 4(d). The threshold energies of these two states are 7.744 and 8.473 eV, and they decay by the transitions $4d\ ^1D_2 \rightarrow 4p\ ^1P_1$ and $5d\ ^1D_2 \rightarrow 4p\ ^1P_1$ via the emission of 636-nm and 463-nm photons, respectively.

Both these states exhibit the b' and c' resonances, which are observed at 11.10 and 11.31 eV for the $4d\ ^1D_2$ state and 11.06 eV and 11.29 eV for the $5d\ ^1D_2$ state. The resonance *a* is not observed clearly for either state. Figs. 4(c) and 4(d) show that these resonances are much better resolved and more prominent in the $4d\ ^1D_2$ excitation function, where the resonances are 15% of the interpolated background compared to 8% for the $5d\ ^1D_2$ excitation function. This was also the case for the study of Shpenik *et al.* [13], whose $4d\ ^1D_2$ state resonance energy data are included in Table I. Another experiment conducted in our laboratory [15] suggests that the *b* resonance, observed here for the $4p\ ^1P_1$ and $4d,5d\ ^3D_{1,2,3}$ states, may also affect the $4d\ ^1D_2$ excitation function. These spin-polarized incident electron Stokes parameter measurements observed a resonance at 10.98 eV, which coincides with the average *b* resonance position of 11.02 eV within the error of both experiments. It is possible that a contribution from the *b* resonance is masked in Figs. 4(a) and 4(b) by the steep rise in photon counts due to the b' resonance. The second resonance observed at 11.33 eV in the Stokes parameters is in excellent agreement with the resonance peak labeled c'. However, the spin-dependent behavior and different resonance shapes apparent in the photon polarization measurement with the lower-energy resolution indicates that it is not straightforward to compare them with the present photon intensity measurements.

In the PCI affected energy region above 11.5 eV, the $4d\ ^1D_2$ and $5d\ ^1D_2$ state excitation functions differ significantly from each other and from the excitation functions of ^3D states with the same *n*. As can be seen in Figs. 4(a) and 4(b), the $4d\ ^1D_2$ photon excitation function shows a broad peak centered around 12.6 eV approximately 1.5 eV wide. We do not consider the weak undulations between 13.2 and 14.2 eV to be statistically significant. On the other hand, there are clearly resolved PCI structures in the $4d\ ^3D_{1,2,3}$ excitation function throughout this energy region, as shown in Figs. 3(a) and 3(b). The binding energies of $4d\ ^1D_2$ and $4d\ ^3D_{1,2,3}$ differ by less than 40 meV, and so one may expect $4d\ ^1D_2$ also to be affected by PCI. The observed lack of structure may perhaps be due to different interference effects. Shpenik *et al.* [13] report three structures in their $4d\ ^1D_2$ state excitation function at 12.45, 14.48, and 14.89 eV, but these are not visible clearly in their published data. In contrast to the $4d\ ^1D_2$ state, the present $5d\ ^1D_2$ excitation function shows three well-pronounced peaks, *S*1 at 11.94 eV, *S*2 at 12.90 eV, and *S*3 at 13.60 eV, followed by indication of another structure *S*4 at 14.16 eV. The positions of these structures are in good agreement with structures observed by Shpenik *et al.* [13]. However, since they were observed clearly for only one state in the present study, these structures cannot be attributed conclusively to PCI and will be excluded from the more detailed analysis to follow.

IV. DISCUSSION

The negative-ion resonances and PCI effects observed here have the comon property that they are both associated with the excitation of one 3*d* electron. They appear at electron impact energies a few eV above the ionization threshold where a number of autoionizing states with a $3d^{10}4p^2$ or $3d^9 4s^2 4p$ electron configuration have been identified [4,7], some of which are forbidden by dipole selection rules. The effects of negative ion resonances and PCI structures on decay photon intensities from different excited states are presented in Tables I–III. The tables are structured to aid understanding of angular momentum effects in negative-ion decay and the exit channel binding energy dependence of the PCI, in this correlation dominated low-energy scattering regime where both discrete and continuum states are open scattering

and decay channels. Negative-ion resonances and PCI will be discussed separately in Secs. IV A and IV B.

A. Negative-ion resonances

In classifying observed negative-ion resonances one first has to consider the assignment of an electron configuration and then an appropriate momentum coupling scheme. For the present resonances, a $3d^9 4s^2 4p^2$ electron configuration has been assigned, as discussed in our previous publications [6,15]. We consider here momentum coupling schemes and the manifold of expected state energies for the $3d^9 4s^2 4p^2$ electron configuration. In the absence of theoretical predictions, a comparison of the resonance energies listed in Table I with spectroscopic data on $3d^9 4s^2 4p^2$ autoionizing states of neutral gallium, which is isoelectronic to Zn^-, will be used as a basis for further interpretation. A more detailed discussion will not be presented without modeling which takes configuration mixing into account, which as noted above is indicated by Mansfield [7] to be essential for reproducing the correct energy ordering of the $3d^9 4s^2 4p$ states.

To determine the most appropriate angular momentum coupling scheme for negative ions with a $3d^9(^2D)4s^2 4p^2$ electron configuration, we consider the following. In the case of a well-defined shell structure, the hole created in the $3d$ orbital would be screened efficiently by the symmetrical charge distribution of two outer $4s$ electrons. So it is likely that the electrostatic interaction between the two excited $4p$ electrons dominates over the interaction of the individual electrons with the ion core. Thus, the momentum state of this electron pair has first to be described using *LS* coupling where the orbital and spin momenta of the two electrons couple to give the total orbital $\vec{L}=\vec{\ell}_1+\vec{\ell}_2$ and total spin $\vec{S}=\vec{s}_1+\vec{s}_2$ momenta. The interaction between the pair of $4p$ electrons and the ion core then determines which scheme describes their momentum coupling most accurately. In full *LS* coupling, as applied to gallium autoionizing states, the orbital and spin angular momenta of the ^2D core couple, respectively, to the $\vec{L}$ and $\vec{S}$ of the $4p$ electron pair. This is a valid approximation as long as the spin-orbit interaction is weaker than the remaining noncentral part of the electrostatic interaction between the ion core and the electron pair.

The energy spectrum and assignments of the $3d^9 4s^2 4p^2$ autoionizing states of gallium [26,27] are shown in Fig. 5. Connerade [26] performed unrestricted Hartree-Fock configuration average calculations using the MCHF72 code of Froese-Fischer [28] and approximate *LS* coupling which are in reasonable agreement with observed transition energies but not always with intensities. The zinc negative ion energies from Table I and the zinc autoionizing states arising from the $3d^9 4s^2 4p$ electron configuration [7,24] are also indicated in Fig. 5. These autoionizing states can be considered as parents of the observed resonances; i.e., the scattered electron can be considered as being bound in the field of one of these states.

When *LS* coupling is applied to the $4p$ electron pair and restrictions imposed by the Pauli principle taken into account, the three states ^1D, ^3P, and ^1S [29,30] can be formed. *LS* coupling of the electron pair to the ^2D ion core leads to the proposed symmetries [27] of observed states of gallium displayed in Fig. 5. Arrows indicate from which electron pair symmetry the observed states are derived, and the doublets resulting from fine structure components are connected with horizontal bars. States are indicated by their configuration and L and S quantum numbers for the core and the electron pair, for example, $3d^9(^2D)4s^2 4p^2(^3P)$, and the term designation $^{2S+1}L_J$ indicates as usual the L, S, and J quantum numbers describing the state overall [27]. While a detailed comparison between the gallium autoionizing and zinc negative-ion energy spectra is not possible due to the limited experimental energy resolution and the possibly large resonance width, both display a similar general pattern. Like the gallium autoionizing states, the zinc resonances are separated into three groups which also display clear evidence of doublet or closely spaced multiplet structure.

Although one would expect that $3d^9 4s^2 4p^2$ zinc negative ions and gallium autoionizing states with the same electron configuration would have a similar energy level structure, complications due to the larger nuclear charge of gallium and the role of spin-orbit interaction in the second momentum coupling step need to be considered. For example, significant spin-orbit effects follow from the prediction [7] of a strongly mixed character for the $3d^9 4s^2 4p$ autoionizing states in zinc. Also, spin-polarized electron measurements by Pravica *et al.* [15] observed a small but nonzero value of the Stokes parameter P_2 for the negative-ion resonance at 11.01 eV, which is a clear signature of spin-orbit interaction. This indicates that an intermediate scheme such as *jLS* may be appropriate to describe the zinc negative-ion resonances.

A variant of *jLS* coupling was applied with success to resonances in noble gases [31]. As for *LS* coupling, the two outer electrons are described in terms of their total orbital $\vec{L}$ and spin $\vec{S}$ angular momentum. Next, either the $\vec{L}$ or $\vec{S}$ of the electron pair couples with the $\vec{j}$ of the core. For noble gas resonances, in line with the situation for excited neutral states, it was assumed that the coupling of $\vec{j}$ and $\vec{L}$ is stronger so that these two couple to form a total angular momentum $\vec{K}$, which in turn couples with $\vec{S}$. Resonance assignment for the noble gases was assisted by high-sensitivity metastable atom excitation function studies, which observed several members of the resonance series. The present zinc experiments only observe one resonance electron configuration, so do not reveal any series regularities.

Finally, we note that the energy separation between the *b* group and *c* group resonance structures is very similar to the 0.337 eV spin-orbit splitting between the $3d^9 4s\ ^2D_{5/2}$ (at 17.171 eV) and $^2D_{3/2}$ (17.508 eV) ion states. The energy separation of resonances within these structures is similar to the 0.105 eV spin-orbit splitting of a $4p$ electron outside a full $3d$ shell—that is, the splitting between the $3d^{10}4p\ ^2P_{1/2}$ (at 15.405 eV) and $^2P_{3/2}$ (at 15.51 eV) ion states. Also, although we have presented a discussion based on distinct electron configurations, it is possible that this concept may not be applicable when describing the energies of zinc autoionizing states. A small admixture of the lowest excited-state configuration $3d^{10}4s4p$ is observed to be essential for correct ordering of the ^3P, ^3D, and ^1P autoionizing states [7]. The strong coupling of the observed resonances to the

$4s4p\ ^3P$ state may indicate that a similar situation occurs in zinc negative ions.

B. PCI effects on the excitation of the $4d,5d,6d\ ^3D_{1,2,3}$ states

Due to the high density of autoionizing states, it is not a trivial task to identify which are associated with the observed PCI structures and to extract information from the observed energy shifts. To gain some insight into which autoionizing states are strongly excited near threshold, we examined ejected electron spectra data [4], taken at an electron impact energy of 16 eV and an ejected electron angle of 60°, combined with autoionizing state energies [7,24]. Of all the spectra taken by Back *et al.* [4], the one used here was obtained under conditions closest to our experiment. Mansfield [7] used the *ab initio* calculations to obtain both the energies and angular momentum composition of the autoionizing states observed by Back *et al.*, and the assignments given here are from this work. The theoretical energies compare well with the autoionizing state energies derived from the ejected electron spectra. Information regarding near-threshold autoionizing state excitation can also be extracted from energy loss spectra obtained using incident electron energies slightly above the autoionizing state energies. However, in this case the energy loss spectra will be complicated by two factors. First, scattered and ejected electrons will have similar energies, and second the shift of scattered and ejected electron energies will smear out energy loss structures, making their identification difficult.

The experiment [4] indicates that the highest ejected electron yield in the energy region of interest here is associated with the decay of autoionizing states arising from the $3d^9 4s^2 4p$ electron configuration. This is true at both low and higher incident electron energies, indicating that the excitation of one inner $3d$ electron into the first unoccupied p orbital has a much larger probability than the excitation of two $4s$ electrons into any combination of higher orbitals. Furthermore, energy loss spectra [5,6,32] indicate that the excitation of one inner $3d$ electron has a similar probability to the excitation of some $3d^{10}4snl$ states. Indeed, these spectra indicate that of the autoionizing states, only the $3d^9 4s^2 4p$ have a significant cross section at an incident energy of 20 eV. Consequently, it would be reasonable to expect states with a $3d^9 4s^2 4p$ electron configuration to be associated with the PCI effects observed here.

The discussion will be restricted to observations of the ^3D states, shown in Fig. 3, for reasons discussed in Sec. III C. One would expect the energy of an autoionizing state associated with a PCI structure to be close to, but not higher than, the onset of the structure in the lowest neutral state in which it is observed. Considering this, autoionizing states which could be associated with the PCI structures were identified from the ejected electron spectra of Back *et al.* [4] (see Table 1 and Fig. 3 of this reference). The relevant autoionizing states and state energies are indicated in Fig. 5. Once possible states have been identified, the relative ejected electron intensities can then be used to assess which of these autoionizing states were the most likely to be associated with the PCI structures. It should be noted, however, that this whole

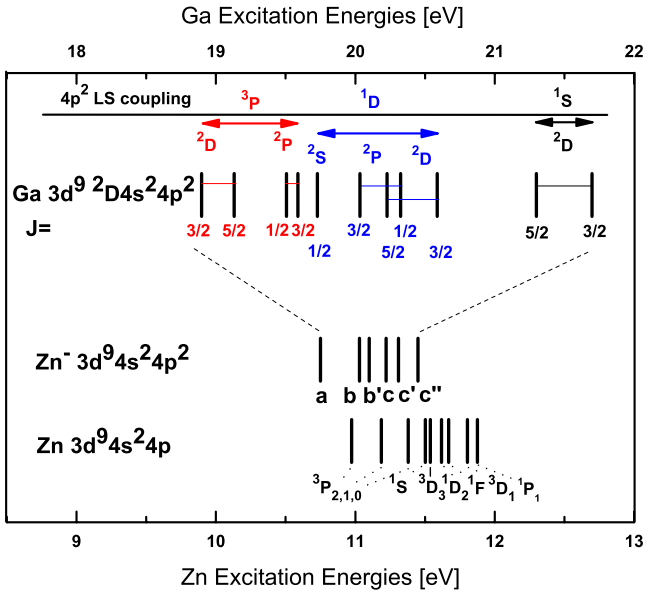

FIG. 5. (Color online) Observed energy levels of Ga, Zn, and Zn^-. Upper energy scale: the $3d^9(^2D)4s^2 4p^2$ autioionizing states of gallium [27]. Assignments are based on the *LS* coupling scheme [26]. Lower-energy scale: zinc negative-ion resonances from Table I and $3d^9 4s^2 4p$ autoionizing state energies [7].

approach assumes that the relative ejected electron intensities and therefore autoionizing state cross sections are not significantly different closer to threshold and at different ejected electron angles, which may not be the case.

From Fig. 3, the onset of the $T1$ and $T2$ structures is 11.64 eV and 12.68 eV, respectively. The $T3$ structure was not clearly resolved in all spectra, so will not be discussed. Below 11.64 eV, the $3d^9 4s^2 4p\ ^3P_{0,1,2}$ states at 10.974, 11.187, and 11.379 eV, respectively, the $3d^{10}4p^2 1S_0$ state at 11.504 eV, the $3d^9 4s^2 4p\ ^3D_3$ state at 11.539 eV, and the $3d^9 4s^2 4p\ ^1D_2$ state at 11.619 eV have been observed in the ejected electron spectra. By far the strongest contribution is from the $3d^9 4s^2 4p\ ^3P_1$ state, the $3d^9 4s^2 4p\ ^1D_2$ state is barely resolved, and the others are approximately one-third to one-sixth of the intensity of the strongest peak.

Considering now the $T2$ structure, in addition to those above the states observed below 12.68 eV in the ejected electron spectra are the $3d^9 4s^2 4p\ ^1F_3$ state at 11.669, the $3d^9 4s^2 4p\ ^3D_1$ state at 11.799, the $3d^9 4s^2 4p\ ^1P_1$ state at 11.884, and the $3d^{10}4p5s\ ^3P_1$ at 12.654 eV. This last state produces a very weak peak in the ejected electron spectra, with an intensity approximately 20 times smaller than that associated with the $3d^9 4s^2 4p\ ^3P_1$ state. The other three states in this group appear to have appreciable cross sections, with their associated ejected electron peaks having intensities between approximately one-quarter and one-half of that for the $3d^9 4s^2 4p\ ^3P_1$ state.

The analysis of Mansfield also shows that most states likely to be associated with the observed PCI structures are strongly mixed. For example, the $3d^9 4s^2 4p$ state at 11.186 eV which produces the largest ejected electron peak has been assigned as 92% ^3P+4% ^1P+3% ^3D. Even stronger mixing is present in the high-angular-momentum

$3d^9 4s^2 4p$ (36% ^1F+33% ^3D+31% ^3F) state which produces the second largest ejected electron peak. Furthermore, the autoionizing states with the largest cross section at higher energies and in photoionization are the $3d^9 4s^2 4p$ (73% ^3D+20% ^1P+6% ^3P)+$3d^{10} 4s 4p$(0.5% ^1P) state at 11.799, and the $3d^9 4s^2 4p$ (73 % ^1P+24% ^3D+1% ^3P) +$3d^{10} 4s 4p$(2% ^1P) state at 11.884 are an admixture of different configurations with large ^3D and ^1P characters for both states. Given this strong mixing, it is uncertain which autoionizing states, or even which components of these states, decay most strongly via the PCI to the neutral states which we observe.

There is another consideration important to this discussion of PCI in zinc: namely, that for near-threshold excitation of the lowest autoionizing states the scattered and ejected electrons will have similar energies. This situation is similar to that where Wannier-type correlations can be expected. In contrast, in most PCI observations to date the ejected electron has a much larger energy and is the electron which gains energy. On the other hand, for example, in a zinc energy loss spectrum taken with an incident energy of 15 eV there would be an overlapping contribution of scattered and ejected electron peaks in the vicinity of the autoionizing state energies. The observed scattered and ejected electron peaks would also be broadened and deformed due to PCI during autoionization.

The present PCI structures are also unusual because the decay of $3d^9 4s^2 4p$ autoionizing states to the $3d^{10} 4snl$ states observed will require a $3d$ core hole to be filled and consequently a previously unexcited $4s$ electron to become active. Several different mechanisms by which this may occur may be envisaged, but we simply note here that the energy and momentum exchange process will involve three electrons, two of which are bound at the start and at the end of the scattering interaction, and large rearrangements of orbital angular momentum. The fundamental principles of large angular momentum transfer in electron scattering from atoms have been discussed by Fano [33], specifically for the case of high-ℓ-state excitation. Subsequently, Fano's arguments were applied to PCI in the excitation of Rydberg states [17] in helium, and angular momentum exchange between outgoing scattered and ejected electrons was also reported in [34]. According to Fano, high values of angular momentum are transfered via a torque which one electron exerts on the other in an interaction lasting for a time comparable to the orbital period of the excited state. Although Fano's analysis applies to ionization in the Wannier regime, the motion of two electrons and the escape or capture of one of them into a bound orbit is the same as reported here and is governed by the same type of correlations. The result essential to the current discussion is that the torque which determines the maximum momentum which one of the electrons can attain depends inversely on the velocity v of the faster electron. This implies a significant difference between the amount of orbital momentum which can be transfered by PCI in zinc compared to helium. The zinc autoionizing states of interest here occur within 2.5 eV of the first ionization threshold. So for near-threshold autoionizing state excitation the ejected electron will have an energy below 2.5 eV, but will be faster than the scattered electron. An order-of-magnitude estimate of the maximum possible exchange of orbital momentum [17,33] gives

$$\Delta J \leqslant e^2/4\pi\epsilon_0 v. \tag{1}$$

For an ejected electron energy of 2 eV, the estimate above gives a value of $\Delta J \leqslant 2.61\hbar$, so up to two units of orbital momentum ($\ell=2$) can be transfered by PCI for any of the autoionizing states considered.

V. CONCLUSIONS

Zinc negative-ion resonances have been observed above the first ionization threshold, and the selective decay of these ions into seven states below the ionization threshold with a range of n, L, and S quantum numbers has been investigated. Relative to nonresonance scattering, the resonance contribution to the observed signal is largest for the $4p\ ^3P_1$ and $4d,5d,6d\ ^3D_{1,2,3}$ states. PCI has been observed to affect the excitation of the higher-energy states studied, and in particular its influence on $4d,5d,6d\ ^3D_{1,2,3}$ state excitation is marked. Because of the structure of zinc, in the incident energy range here Wannier-type correlations and a large PCI orbital angular momentum transfer are possible. The negative-ion resonances and PCI observed here are associated with the excitation of a $3d$ electron, which causes significant electron correlations both within the zinc target atom and between the active electrons.

Further experiments with spin-polarized electrons can test the role of spin-orbit and exchange scattering in the resonance region, and angle differential electron excitation function measurements can provide information regarding the resonance symmetry and predominant partial waves to aid the resonance assignments. Both these types of experiments are in progress in our laboratory.

ACKNOWLEDGMENTS

This work was supported by the Australian Research Council and the University of Western Australia. The apparatus was constructed and maintained by Steve Key and other staff of the UWA Physics mechanical workshop.

[1] D. H. Yu, P. A. Hayes, J. F. Williams, and J. E. Furst, J. Phys. B **30**, 1799 (1997).
[2] G. V. Marr and J. M. Austin, J. Phys. B **2**, 107 (1969).
[3] R. Kuntze, N. Böwering, M. Salzmann, U. Heinzmann, and N. L. S. Martin, J. Phys. B **29**, 1025 (1996).
[4] C. G. Back, M. D. White, V. Pejčev, and K. J. Ross, J. Phys. B **14**, 1497 (1981).
[5] B. Predojević, D. Sević, V. Pejčev, B. P. Marinković, and D.

Filipović, J. Phys. B **36**, 2371 (2003).
[6] S. Napier, D. Cvejanovic, J. F. Williams, and L. Pravica, J. Phys. B **40**, 1323 (2007).
[7] M. W. D. Mansfield, J. Phys. B **14**, 2781 (1981).
[8] G. C. King, F. H. Read, and R. C. Bradford, J. Phys. B **8**, 2210 (1975).
[9] S. J. Buckman and C. W. Clark, Rev. Mod. Phys. **66**, 539 (1994).
[10] J. P. Sullivan, P. D. Burrow, D. S. Newman, K. Bartschat, J. A. Michejeda, R. Panajotovic, M. Moghbelalhossein, R. P. McEachran, and S. J. Buckman, New J. Phys. **5**, 159.1 (2003).
[11] I. P. Zapesochnyi and O. B. Shpenik, Sov. Phys. JETP **23**, 592 (1966).
[12] O. B. Shpenik, I. P. Zapesochnyi, V. V. Sovter, E. E. Kontrosh, and A. N. Zavilopulo, Sov. Phys. JETP **38**, 898 (1974).
[13] O. B. Shpenik, M. M. Erdevdy, and J. E. Kontros, Radiat. Phys. Chem. **76**, 587 (2007).
[14] P. D. Burrow, J. A. Micheida, and J. Comer, J. Phys. B **9**, 3225 (1976).
[15] L. Pravica, D. Cvejanovic, J. F. Williams, and S. A. Napier, Phys. Rev. A **75**, 030701(R) (2007).
[16] O. Zatsarinny and K. Bartschat, Phys. Rev. A **71**, 022716 (2005).
[17] T. van Ittersum, H. G. M. Heideman, G. Nienhuis, and J. Prins, J. Phys. B **9**, 1713 (1976).
[18] R. B. Barker and H. W. Berry, Phys. Rev. **151**, 14 (1966).
[19] R. Morgenstern, A. Niehause, and U. Thielmann, J. Phys. B **10**, 1039 (1977).
[20] P. J. M. van der Burgt, J. van Eck, and H. G. M. Heideman, J. Phys. B **18**, 999 (1985).
[21] W. van de Water and H. G. M. Heideman, J. Phys. B **13**, 4663 (1980).
[22] M. Y. Kuchiev, J. Phys. B **30**, 3499 (1997).
[23] S. A. Napier, D. Cvejanovic, J. F. Williams, and L. Pravica, Phys. Rev. A **78**, 022702 (2008).
[24] NIST, http://physics/nist/gov (database).
[25] H. G. M. Heideman, T. van Ittersum, G. Nienhuis, and V. M. Hol, J. Phys. B **8**, L26 (1975).
[26] J. P. Connerade, Proc. R. Soc. London, Ser. A **354**, 511 (1977).
[27] Y. Ralchenko, A. E. Kramida, and J. Reader, http://physics.nist.gov/asd3
[28] C. Froese-Fischer, Comput. Phys. Commun. **6**, 119 (1972).
[29] G. Herzberg, *Atomic Spectra and Atomic Structure* (Dover, New York, 1944).
[30] H. G. Kuhn, *Atomic Spectra* (Longman, London, 1971).
[31] F. H. Read, J. N. H. Brunt, and G. C. King, J. Phys. B **9**, 2209 (1976).
[32] S. Trajmar and W. Williams, in *Physics of Ionized Gases, Proceedings of Invited Lectures*, edited by B. Navinsek (J. Stefan Institute, Ljubljana, 1976).
[33] U. Fano, J. Phys. B **7**, L401 (1974).
[34] W. van de Water and H. G. M. Heideman, J. Phys. B **14**, 1065 (1981).